

Short Papers

Automatic Couplings With Mechanical Overload Protection for Modular Robots

Christoph H. Belke  and Jamie Paik 

Abstract—This paper presents an automatic coupling mechanism with mechanical overload protection for use in modular robotic systems. The genderless coupling incorporates a novel safety mechanism that disengages two modules at a predefined torque threshold. Several key design aspects allow the minimalist coupling to contain all functionalities within a compact cylindrical space. A detailed analytical model of the overload protection mechanism is validated by testing two materials and fabrication methods. We further present a functional prototype of the coupling with a demonstration of two modular robots driving toward one another, automatically connecting and disconnecting, detecting the connection, communicating in the process, and sensing the angle between them. The coupling as well as the embedded technologies and mechanisms present essential steps toward enabling fully self-reconfigurable robots combining modular and origami features, while advancing the process of introducing modularity into a wide range of robotic systems.

Index Terms—Coupling mechanisms, mechanical overload protection, origami robots, self-reconfigurable modular robots.

I. INTRODUCTION

Reconfigurable modular robots are versatile systems consisting of multiple entities that, in combination, can change their shape and function depending on the task and environment at hand. In our recent work [1], we introduced a new type of reconfigurable modular robot that merges the fields of modular and origami robots: Mori, a modular origami robot. A modular origami robot has the low profile, simplicity, and reconfigurability inherent to origami robots, as well as the versatility and adaptability of modular robotic systems. In this paper, we further explore the possibilities of modular origami robots by presenting a novel automated coupling mechanism that greatly extends the robot's capabilities and provides solutions to a number of key concerns in modular systems in general.

The coupling of a modular robot is one of the critical aspects that define the system's characteristics and behavior, while its design poses significant challenges [2]. Given a particular architecture of the

Manuscript received March 19, 2019; accepted March 24, 2019. Date of publication March 27, 2019; date of current version June 14, 2019. Recommended by Technical Editor P. Ben-Tzvi. This work was supported in part by the Swiss National Science Foundation START Project and in part by the Swiss National Centre of Competence in Research in Robotics. (Corresponding author: Jamie Paik.)

The authors are with the Reconfigurable Robotics Lab, École Polytechnique Fédérale de Lausanne, 1015 Lausanne, Switzerland (e-mail: christoph.belke@epfl.ch; jamie.paik@epfl.ch).

This paper has supplementary downloadable material available at <http://ieeexplore.ieee.org>, provided by the authors. There is a video associated with the publication.

Color versions of one or more of the figures in this paper are available online at <http://ieeexplore.ieee.org>.

Digital Object Identifier 10.1109/TMECH.2019.2907802

overall system, the coupling must fulfill specific requirements determined by degrees of freedom (DoFs), functionalities, and mechanical design. Couplings can either be gendered [3], with distinct sets of complementary features and reduced functionality, or genderless (hermaphroditic), such that any side of one module can connect to any side of another [4]–[6]. Genderless couplings greatly extend the reconfigurability of a modular system but are generally more bulky and complex. Various coupling methods have been proposed, including mechanical [7], magnetic [8], solder-based [9], and pneumatic [10], with the majority utilizing either mechanical or magnetic systems [11].

Magnetic connectors have been implemented as passive couplings using permanent magnets [12], as a guide during the reconfiguration process [13], and as active couplings using electromagnets [14]. To overcome the high power consumption of electromagnets, semipermanent magnets have been used as a semipermanent interface [15]. Magnetic connectors are a relatively simple solution and fulfill various requirements of couplings such as automatic alignment. However, the low strength provided is oftentimes a disqualifying characteristic as it must be balanced with the ability to disengage modules and misalignment under load. Mechanical couplings are more common in self-reconfigurable systems [14] and are usually based on hooks or latches. While they are generally more complex than magnetic couplings, they offer more design freedom for the embedded mechanisms and their specifications. Their components are most commonly driven by dc motors although some systems utilize shape-memory alloy (SMA) actuators [16]. Many mechanical couplings also have self-alignment features that center connectors during the docking process [17]. Some mechanical couplings are further able to perform single-sided disconnects when a module fails [5].

Besides a mere physical connection, couplings of modular robots provide the only physical interface to communicate with and sense neighbors. While many systems utilize wireless communication [14], a physical communication stream can provide a simple way to identify neighbors and their orientation [5]. Such a connection can also serve to synchronize neighbors and validate their status during locomotion of multiple modules [2] and when multiple units drive the same joint.

Each type of modular robot comes with a distinct set of challenges that depend largely on the overall design of the system and can vary greatly. In most modular robots, the coupling mechanism is separated from any active DoF that changes the robots morphology. By contrast, in a system of lightweight quasi-two-dimensional (2-D) modules that reconfigures by folding into three-dimensional (3-D) structures [1], [18], [19], the coupling axis is also the active folding axis between two modules. The coupling mechanism must, thus, be fully integrated within the actuation mechanism of the folding link, while maintaining a compact slender architecture. The mechanism presented herein has a specific design resulting from the unique requirements of a

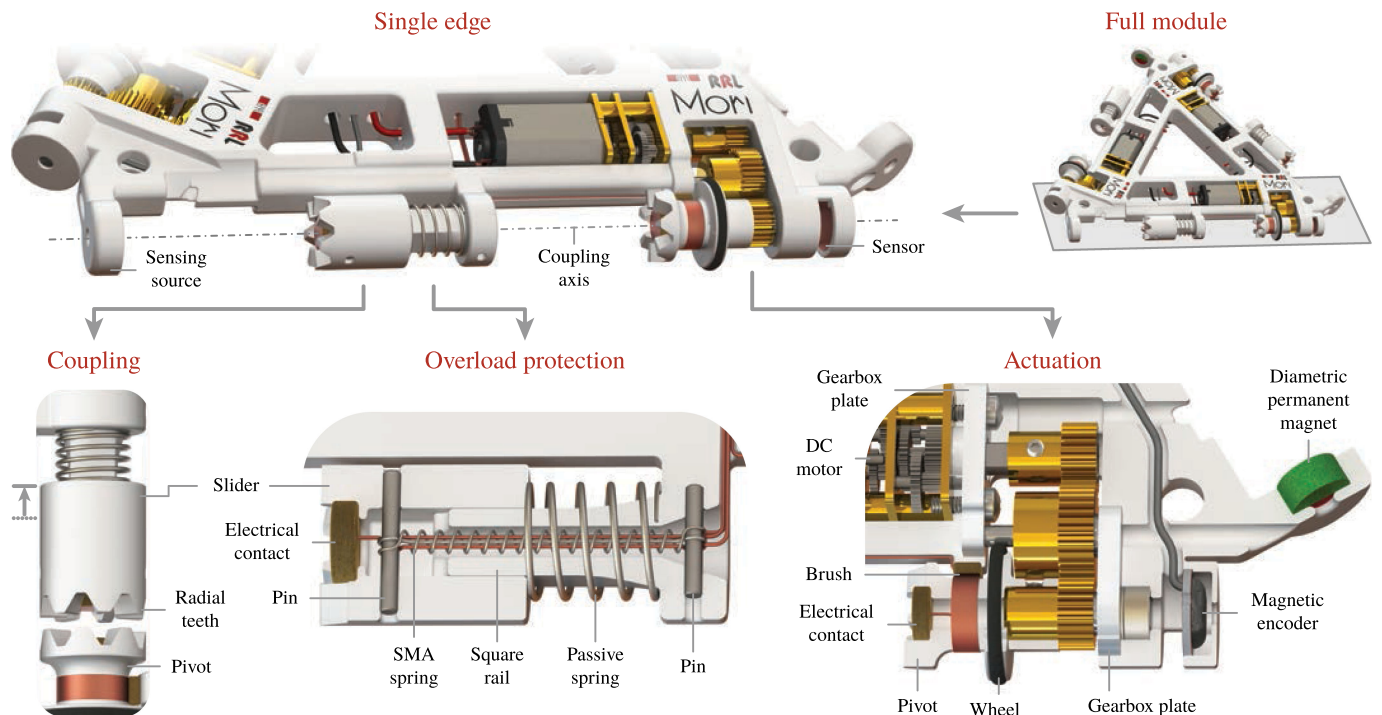


Fig. 1. Design overview of the automatic coupling mechanism with mechanical overload protection. Top: visualization of a whole module (excluding electronics) and a single edge. Bottom: visualization of the coupling, a detailed section view of the overload protection, and an actuation system.

modular origami robot. Its functionalities and novel features, however, are applicable to a large spectrum of modular and reconfigurable systems.

Due to the large number of DoFs in modular robotic systems, individual modules are prone to damage as small forces are amplified through kinematic chains and singularities. More complex single-purpose robots generally employ an abundance of sensors, both external and within the drive system, to ensure that the system's limits are not exceeded. This, however, is not feasible in multi-robot systems due to the added complexity of individual modules, the necessary computational power, and the remaining danger from failure of the control system. In this paper, we propose the use of mechanical overload protection features embedded into each active DoF of a module. Such a mechanism does not interfere with the robots' functionality during normal operation and, thus, does not weaken the robot. Instead, it intervenes only when a force threshold is surpassed, outside of the normal operating conditions. Mechanical overload protection has previously been proven useful in human-robot interaction [20] and damage prevention [21] in humanoids. Modular robots with magnetic interfaces automatically have some degree of overload protection built in, as the coupling disengages when magnetic forces are exceeded. There is, however, a tradeoff between the strength of the coupling, and hence the ability to build larger structures, and the maximum force required to disengage modules. In this paper, we present a novel overload protection mechanism for mechanical couplings that does not interfere with the system during normal operation and, at the same time, ensures that no excessive forces are present.

The main contributions of this paper are the following:

- 1) an automated, self-centering, and genderless coupling for modular robots using SMAs with a low profile, absolute position sensing, and synchronized actuation;
- 2) design, modeling, and experimental validation of a novel mechanical overload protection mechanism for use in modular robotic systems;

- 3) a functional prototype and validation of the automatic coupling mechanism with mechanical overload protection, incorporating connection detection, synchronization, and angular sensing.

II. COUPLING DESIGN

Taking full advantage of modular robots requires each module to be equipped with an automatic coupling mechanism allowing the system to self-assemble and reconfigure into any desired configuration. The coupling must incorporate various features that ensure full functionality of the system such as sensing and actuation of the connection mechanism and any associated DoFs. Additional features may be required depending on the overall design of the system and any imposed constraints. In this section, we discuss a variety of coupling elements and present a design for a modular origami robot, depicted in Fig. 1, that provides the technological building blocks for a range of modular robotic systems.

A. Mechanical Design

A modular robotic system exhibits the greatest flexibility in terms of reconfiguration and module allocation if any edge or face of a module can connect to any other. This can be achieved by incorporating both male and female coupling features into each edge or face, resulting in a genderless (or hermaphroditic) mechanism. Each edge in our design is identical and contains all functional features of the genderless mechanism, as shown in Fig. 1.

A modular origami robot has a quasi-2-D structure with hinges that enable origami-like folding about the coupling axis. In order to maintain a low thickness, all components that cannot be moved away from the coupling axis must be contained within a cylinder of a diameter equal to the device's thickness. This includes actuation elements of the coupling and of the rotational DoF, sensing of the angle, and electrical connections. The design of our coupling mechanism incorporates various elements that extend the capabilities of modular origami robots.

In order to incorporate these features and to reduce the cost of a single module, the overall size compared to our previous prototype [1] is 67% larger, while maintaining the same slenderness ratio. The length of the coupling axis is 133 mm, and the thickness of the design is 10 mm. The main body of a module is fabricated using a multijet 3-D printer (Objet Connex 500), allowing us to incorporate detailed features and to reduce the number of parts. The mechanical design of the coupling mechanism includes the following features.

1) Coupling Mechanism: The first version of our modular origami robot could only be coupled manually with a spring-loaded pin and only when modules were at 180° to one another. In this design, we overcome these limitations by using a similar mechanism with a retractable element with a new approach, as shown in the coupling illustration in Fig. 1. A retraction-based coupling mechanism switches between two states during a coupling process: one state allowing for coupling and decoupling and the other ensuring a steady connection between modules. Since a module is likely to be in the latter state most of the time, whether it is connected to another module or not, it should be designed to minimize, or eliminate, power consumption in this state. We employ an SMA spring, providing a contractile force when heated, to retract the coupling element to an open state. The use of a joule-heated SMA actuator allows us to greatly simplify the retraction mechanism, minimize its size compared to traditional actuators, and eliminate power consumption when closed.

The coupling element, or slider, runs on a rail of square cross section attached to the main body, which allows sliding along the coupling axis but blocks rotation. A passive spring placed around the square pin ensures that the coupling returns to a closed state once the SMA spring cools down and loses its contractile force. The maximum extension is restricted by a string between the coupling element and the base of the square shaft. These design elements are depicted in the overload protection illustration in Fig. 1.

The front face of the coupling element has specially designed radial teeth, the design of which is covered in more detail in Sections II-A3 and III. The teeth of the coupling element engage with identical teeth on a pivot of another module and, thus, transmit rotational actuation. A radial design not only ensures a smooth mesh during operation, it also makes the coupling elements self-centering. When the distance between the axes of two modules is within a certain error band, the axes automatically align during the coupling process. This misalignment tolerance is addressed in Section IV.

2) Actuation: In order to minimize the size of a module, the rotational actuator is embedded in the main body of the module and away from the coupling axis. Three gears transmit the torque from the motor to a pivot on the coupling axis. The actuator is a dc motor with a 297.92:1 reduction ratio from Pololu, and the three gears have a module of M0.3 with 20, 30, and 20 teeth, respectively. The gearbox is precisely located and reinforced using two machined polyacetal (POM) plates, one on each side of the gears. The motor is mounted to one of the plates, the shaft of the middle gear is mounted between both plates, and the final gear holding the pivot with radial teeth is fixed to a cantilevered shaft held by two bearings, one of which is press-fit into the second plate. The actuation mechanism is shown in Fig. 1.

A single module is mobile on flat surfaces when no other module is connected to it, thanks to a wheel incorporated into each pivot. Two modules can, thus, drive toward one another, retract the coupling mechanisms, align their axes, and successfully couple without user intervention. When a configuration of multiple modules is assembled, the wheels of unconnected edges can also be used to drive the overall assembly.

3) Overload Protection: We have developed a mechanical overload protection mechanism to protect the mechanical assembly from

damage. This mechanism disengages two connected modules when the coupling exceeds a torque threshold that is defined by a number of easily adjustable design parameters. The overload protection is incorporated into the design of the coupling such that it shares most of the mechanical features with the retraction mechanism. The two engaging pieces of the coupling, namely, the pivot and the slider shown in Fig. 1, have radial teeth with angled faces such that a torque applied to the coupling also produces an axial force away from the coupling interface. When this axial force overcomes the frictional forces both on the teeth and between the slider and the square rail, the slider moves to an open state. A detailed analysis of this mechanism is presented in Section III.

B. Electronics and Control

An automatic coupling for modular robots not only requires an actuated mechanism to connect to another module, it must also be able to detect whether a connection is made, active, or lost. When coupled, a module must furthermore be aware of its state relative to the connected module. These requirements are addressed in our design as follows.

1) Sensing: As soon as a connection between two modules is made, each module must be aware of the absolute angle between them. The sensing source can, therefore, not be on the same module as the corresponding sensor, as this would only give relative changes in rotation. We use a cylindrical diametric magnet fixed inside the housing, with the same orientation in each module. An absolute magnetic encoder (AS5048B from AMS) on another module can then sense the angle between two modules as soon as their axes are aligned.

2) Synchronization: Since all sides of a module are identical, there are two actuators driving the same link when two modules are connected. It is vital to synchronize this actuation in order to avoid an increase in power consumption and potential damage to the drive mechanism. We have incorporated electrical connections into the coupling elements, the slider and the pivot, with one input and one output for each side of a module, as shown in Fig. 1. It consists of a cylindrical sponge that compresses to ensure a stable contact and a copper layer glued to the surface. Since the pivot can rotate continuously, an additional brush is used to connect the electrical contact of the pivot to the controller. This brush also consists of a sponge and a copper layer that is in contact with a copper strip attached to the outside of the pivot. A communication protocol based on interrupts has further been developed based on serial communication allowing a module to detect when another module is connected or disconnected, as well as to synchronize the actuators controlling the angle between them.

III. OVERLOAD PROTECTION MECHANISM

The novel overload protection mechanism introduced in this paper presents a simple and compact method of preventing damage to robotic joints. It is integrated into the coupling mechanism of our modular origami robot, requiring no additional components, and obtains its functionality from a special parametric design. The mechanism automatically disengages the coupling between two robots when the applied torque exceeds a predefined threshold, which lies outside of the normal working conditions of the robot. This threshold can be modified through a single design parameter such that the mechanism is easily adjusted toward a multitude of applications, scales, and user groups. In this section, we provide a detailed analysis of this overload protection mechanism by modeling its behavior and testing multiple parameters, materials, and fabrication methods.

A. Modeling

The overall concept of the mechanism is based on a number of functional requirements and fuses existing mechanical features and

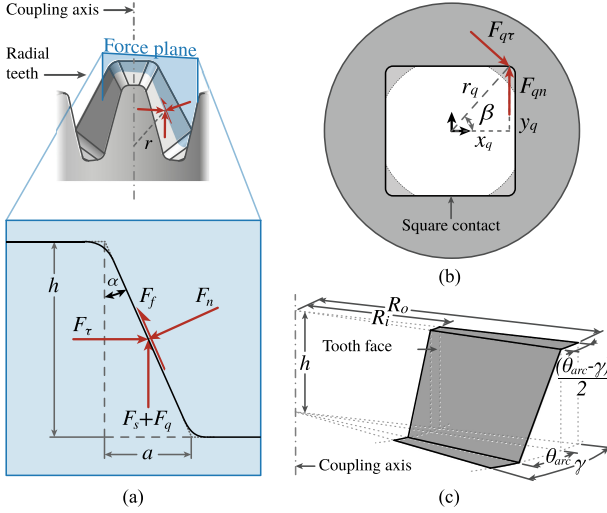


Fig. 2. Modeling diagrams for the two contact points in the overload protection model. (a) shows the force plane of a tooth face and the forces acting on it. (b) shows the contact forces between the slider and the square rail. (a) and (b) are used to calculate the torque threshold τ_{thresh} . (c) Radial tooth design schematic. The tooth face is the interaction surface between two teeth. The design parameters in this schematic can be altered to change the torque at which the coupling disengages.

functions. The actual coupling consists of two complimentary pieces with identical radial teeth that mesh to transmit rotational actuation. Below the predefined torque threshold, the coupling behaves like a positive clutch, which couples two pieces by mechanical interference and cannot slip. Thus, the mechanism does not weaken the robot or hinder performance during normal operation. When the torque threshold is reached, however, the slider retracts and causes the coupling to disengage. This effect comes from the angular design of the teeth producing an axial force on the slider, which overcomes frictional and spring forces at a threshold.

The design is centered around a variable torque threshold, τ_{thresh} , which is dependent on a number of design parameters. In the following analysis, we develop an expression for τ_{thresh} such that it can be adjusted by modifying a single parameter. For this purpose, we first consider the geometry of the radial teeth, depicted in Fig. 2(c). The teeth have similarities to those of a Hirth joint, a locked mechanical coupling for shafts, although with an altered design and a different purpose. The faces of each tooth span between two radial lines, resulting in a varying angle of the face along the radius, unlike a Hirth joint. This allows for a planar, rather than a conical, design of the coupling mesh. The varying angle of the face is one of the key factors determining the torque threshold and is dependent on the tooth arc angle θ_{arc} and the height of the tooth, h . The angle spanned by half a tooth, γ , is defined by the number of teeth, n , as $\gamma = \pi/n$, limiting the maximum value of θ_{arc} . The contact area between two teeth is then fully defined through the inner and outer radii, R_i and R_o , respectively.

Considering the overall geometry of the radial teeth, we can establish a force plane, orthogonal to the radius, to evaluate the interaction forces between two teeth, illustrated in Fig. 2(a). The force plane creates a cross-sectional profile at radius r with an angle α between the face and the coupling axis given by $\tan(\alpha) = a/h$, where a is the distance between the two radial lines, fully defining the face at radius r . Using the equilibrium of forces both along the surface and orthogonal to the surface, we can establish expressions for the frictional force between two teeth, F_f , given by

$$F_f = F_\tau \sin(\alpha) - (F_s + F_q) \cos(\alpha) \quad (1)$$

TABLE I
GLOBAL DESIGN PARAMETERS

Parameter	Symbol	Value
Number of teeth	n	7
Tooth height	h	2 mm
Inner radius	R_i	2.5 mm
Outer radius	R_o	5 mm
Pre-load distance	x_s	5.4 mm
Spring stiffness	k	0.33 N mm ⁻¹

and the reaction force resulting from the opposite tooth, F_n , given by

$$F_n = F_\tau \cos(\alpha) + (F_s + F_q) \sin(\alpha) \quad (2)$$

where F_τ is the force orthogonal to the radius resulting from the torque τ applied to the coupling such that $\tau = rF_\tau$, F_s is the force exerted by the passive spring, and F_q is another frictional force resulting from a force on the square rail due to the applied torque.

The spring force F_s is given by $F_s = kx_s$, where k is the spring stiffness and x_s is the preloaded distance, while the frictional force from the square rail, F_q , can be determined as follows. Due to a small clearance between the slider and the square rail, the torque applied to the coupling can be translated to a force toward the corner of the square cross section, $F_{q\tau} = (r/r_q)F_\tau$, as shown in Fig. 2(b), where r_q is the distance between the point where $F_{q\tau}$ is applied and the center of the slider. The resulting reaction force F_{qn} creates a frictional force that resists the motion of the slider, F_q , which can be approximated using Coulomb friction as

$$F_q = \mu \frac{r}{r_q} F_\tau \cos(\beta) \quad (3)$$

where μ is the static coefficient of friction and β is the angle between the force $F_{q\tau}$ and the normal to the surface.

We can now find an expression for the torque threshold τ_{thresh} by relating (1) and (2) using Coulomb friction and (3), given by

$$\tau_{\text{thresh}} = \frac{F_s (\mu \sin(\alpha) + \cos(\alpha))}{\sin(\alpha) - \mu \cos(\alpha) - \lambda \cos(\alpha) - \mu \lambda \sin(\alpha)} \quad (4)$$

where the tooth arc angle θ_{arc} can be related to the torque threshold using the face angle $\alpha = \arctan(2r \sin(\theta_{\text{arc}}/2)/h)$, and $\lambda = \mu(r/r_q) \cos(\beta)$ is used for simplification.

We have chosen the tooth arc angle θ_{arc} as the key design parameter, keeping all other parameters constant. Given a desired torque threshold τ_{thresh} and specific design, we can adjust θ_{arc} to yield the required behavior of the mechanism.

B. Testing

Given the above model, we can design the overload protection mechanism by choosing parameters that meet the overall specifications of the robot and adjusting θ_{arc} to yield the desired torque threshold. The global design parameters established during the design process presented in Section II are presented in Table I.

In order to verify both the feasibility of the overload protection mechanism and the model thereof, we utilized two materials and fabrication methods to manufacture test pieces. One set of test pieces was made out of VeroWhite using a multijet 3-D printer, while the other set was CNC-machined out of polyacetal (POM). The VeroWhite pieces were printed with a glossy finish and a layer height of 16 μm , and the POM pieces were CNC-machined with a resolution of 15 μm . The remaining modeling parameters for the two materials measured after fabrication are given in Table II.

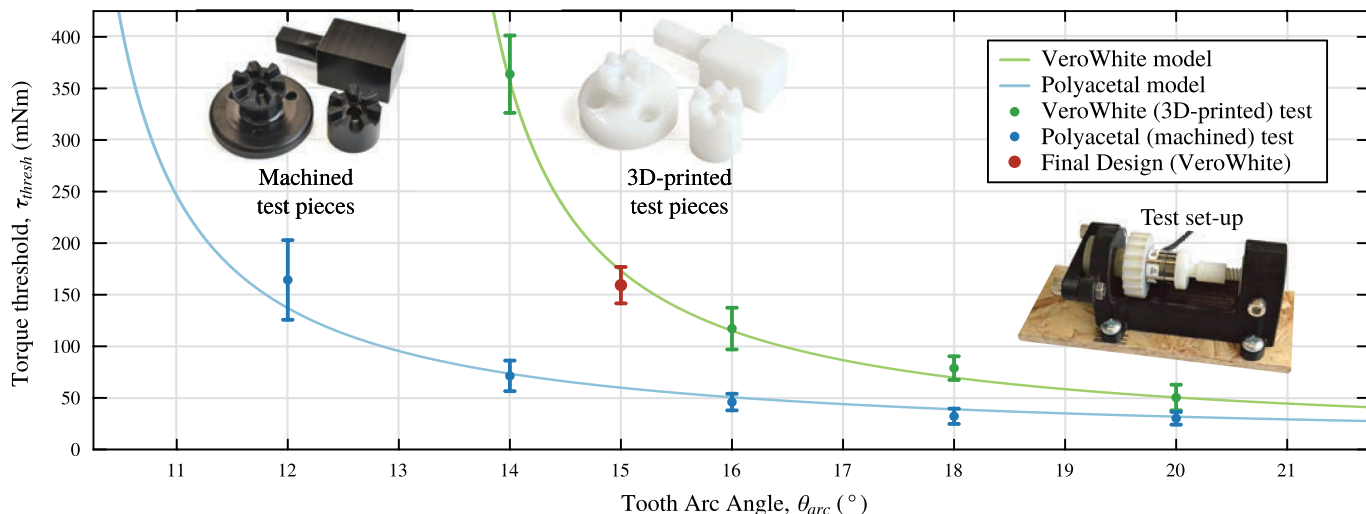


Fig. 3. Results obtained from modeling the overload protection mechanism and from testing the model on two materials and fabrication methods. The torque at which the coupling disengages is plotted against the tooth arc angle, θ_{arc} , a design parameter of the radial teeth. VeroWhite was 3-D printed and used in the final design of the coupling mechanism, while the polyacetal pieces were CNC-machined.

TABLE II
MATERIAL- AND FABRICATION-DEPENDENT PARAMETERS

Parameter	Symbol	VeroWhite	POM
Friction coeff.	μ	0.25	0.19
Slider angle	β	50.6°	52.3°
Slider radius	r_q	2.95 mm	2.77 mm

We fabricated six test pairs and one square contact for each material with arc angles increasing in 2° intervals from 10° to 20°, as well as one final test pair that matches the desired torque threshold using the 3-D printer with an arc angle of 15°. The samples were placed in a test frame that mimics the placement within a coupling with a manual drive wheel for the pivot. A torque sensor (ATI Nano 17) was attached to the pivot such that the torque could be gradually increased until the overload protection was triggered and the test pieces disengaged. This was repeated at least 20 times per sample set to obtain an average value for the real torque threshold.

Fig. 3 shows the test results for the two sets of test pieces, the corresponding modeling results from Section III, sample test pieces, and the testing setup. The modeling result approaches asymptotically at 13.08° and 9.76°, reflecting the self-locking condition that occurs when the axial force produced by the torque acting on the angled teeth can no longer overcome the frictional forces acting on the slider. This self-locking condition was confirmed during the test as the mechanism did not disengage up to the limit of the torque sensor (0.5 N·m) at arc angles of 10° and 12° for the 3-D-printed test pieces. The machined test pieces with an arc angle of 10° did not disengage up to the limit of the torque sensor, since the modeled threshold is several times larger. The remaining test pieces confirm the expected behavior of the mechanism, disengaging at values close to the predicted torque thresholds. Although errors in the torque threshold of 10–20% are significant, the test validates the functionality and efficacy of the overload protection mechanism.

While these errors are acceptable in our implementation and can be accounted for in the design, some applications may demand more precise threshold values from the mechanism, which can be achieved in a number of ways. Errors become larger as the value for the arc angle approaches the self-locking condition, as small variations in

geometry and surface finish have a bigger impact on the torque threshold. Therefore, designing the system such that the desired torque threshold occurs at an arc angle value significantly higher than the self-locking condition improves the effective precision. Alternatively, mechanical improvements can reduce errors such as tightening tolerances in the machining process, adjusting the CNC cutting profile to better reflect the path of moving elements, or using different materials for interfacing parts in order to improve sliding properties. 3-D-printed pieces, although used by the authors in this instance for ease of manufacture, are less predictable due to the quality of the UV-cured glossy surface finish.

The desired torque threshold for the final design of our modular origami robot is determined by the recommended maximum torque value of the dc motors, given as 25 oz-in (or 177 mN·m) by the manufacturer. This corresponds to a tooth arc angle of 15°, which was verified during testing, as shown in Fig. 3. In case the intended application, user group, or motor specifications for the coupling change, the torque threshold can easily be adjusted by replacing the two coupling elements in each hinge of the robot.

IV. IMPLEMENTATION

Following the modeling of our proposed mechanism, this section presents our prototype of the automatic coupling and a demonstration thereof. The design presented in Section II has been implemented in two identical of the coupling in the form of a single edge of a modular origami robot, shown in Fig. 4. Each prototype is controlled using Arduino Uno running identical programs with no physical connections between them. The only communication between the controllers occurs through the electrical contact within the coupling.

To test the full coupling mechanism, we placed the two prototypes opposite to one another with their axes aligned, but a small distance away from each other, as shown in the initial state in Fig. 4. This ensures that the prototypes engage when moving forward, since a single edge only has one DoF while moving (a full module has three DoFs in locomotion). Once aligned, a coupling sequence is initiated consisting of retracting the slider (frame 1), moving forward (frame 2), and releasing the slider (frame 3). If a connection is not detected immediately, the pivots start rotating back and forth until an electrical contact is made, accounting for the flat face at the end of each tooth. Once two modules

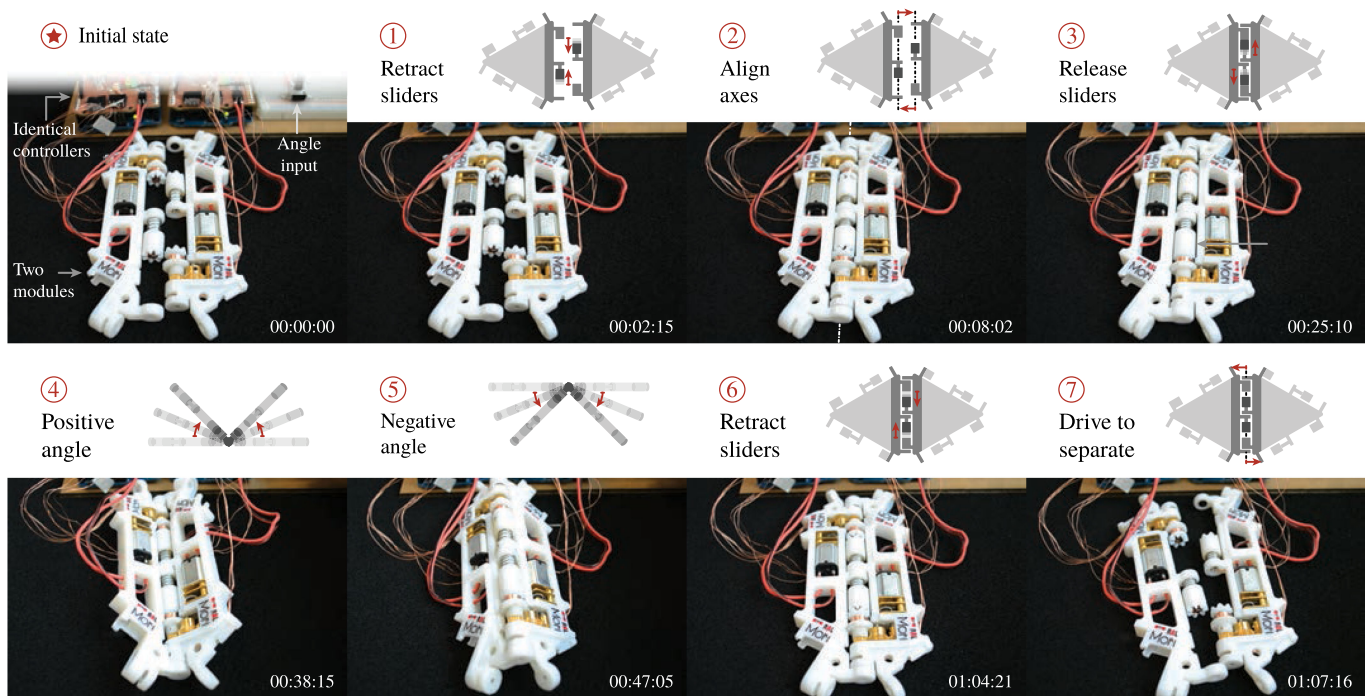


Fig. 4. Testing of the coupling mechanism with key frames showing main steps in the process. The coupling sliders are first retracted, and two modules drive toward one another to align the coupling axes. The coupling then engages, and the angle between the modules is set using a potentiometer. During the uncoupling process, the pins are again retracted, and the modules drive away from each other.

TABLE III
MISALIGNMENT TOLERANCES

Direction	Value	Percentage
Radial	± 2.5 mm	± 25 %
Axial	+1.2 mm, -0.5 mm	+1.1 %, -0.5 %
Angular	$\pm 3^\circ$	n/a

are coupled and have confirmed synchronization, both modules actively maintain the desired angle of the coupling through closed-loop control (frames 4 and 5). In our test, we ensure that both modules receive the same desired angle by using a single potentiometer connected to both module controllers. The position of the potentiometer then determines the absolute angle of the coupling. In order to disengage the modules, a decoupling sequence is initiated consisting of returning to an absolute angle of zero, retracting the sliders (frame 6), and moving away from each other (frame 7).

We further tested the mechanism ability to account for misalignment of two couplings by placing the two edges onto separate rigs and increasing misalignment radially and in the angle between the coupling axes. The results from the misalignment test are summarized in Table III. The misalignment tolerance in the axial direction results from the travel of the slider and additional chamfers and clearances that guide the couplings. The relatively large tolerance of 25% in the radial direction, the most critical for a modular origami robot, arises from the self-centering design of the teeth, as outlined in Section III.

V. DISCUSSION

The design of couplings for modular robots presents various challenges and requirements that must be solved and fulfilled to create fully

functional self-reconfigurable systems. These comprise, among others, a robust mechanism design, actuation, and sensing of the connection and associated DoFs, ease of coupling and alignment, as well as communication and synchronization. In this paper, we present a genderless automatic coupling mechanism with embedded mechanical overload protection that overcomes some of the hurdles associated with modularity in a wide range of robotic systems. The coupling contains various unique features that can be applied to other systems individually or as a whole to improve the reconfigurability of robots.

The coupling utilizes SMA actuators to automate the docking process and dc motors to actuate the rotational DoF. A special electronic connection embedded into the coupling not only enables each module to detect the state of the coupling and to gather information about the neighboring module, but also serves as a means of synchronization. Mechanical overload protection incorporated into the coupling protects the robots from damage. It consists of a friction-based positive clutch mechanism that is triggered when a predefined torque threshold is reached. Thanks to a parametric self-centering design, this threshold can easily be adjusted to meet the varying requirements. Along with the design, modeling, and testing of the proposed coupling, we present a working prototype thereof. Using a single edge of two modules, we demonstrate a coupling process with automatic coupling and decoupling, detecting and synchronizing the connection, as well as closed-loop control of the rotational DoF. We furthermore validated the self-centering design by testing misalignment tolerances.

The coupling mechanism represents one of the advancements necessary to realize a fully functional modular origami robot. While the design of the mechanism is directed toward modular origami robots, our approaches to actuation, coupling, overload protection, sensing, and communication represent building blocks that can be used to incorporate modularity into other robotic systems. We thus hope that the work presented herein will promote the development and presence of reconfigurability and modularity in various fields of robotics.

REFERENCES

- [1] C. H. Belke and J. Paik, "Mori: A modular origami robot," *IEEE/ASME Trans. Mechatronics*, vol. 22, no. 5, pp. 2153–2164, Oct. 2017.
- [2] K. Støy, "Reconfigurable robots," in *Springer Handbook of Computational Intelligence*. Berlin, Germany: Springer, 2015, pp. 1407–1421.
- [3] C. Yuan, R. Yin, W. Zhang, and G. Chen, "A new under-actuated resilient robot," in *Proc. IEEE Int. Conf. Syst., Man, Cybern.*, Banff, AB, Canada, Oct. 2017, pp. 1202–1207.
- [4] S. Hong, W. Lee, K. Kim, H. Lee, and S. Kang, "Connection mechanism capable of genderless coupling for modular manipulator system," in *Proc. 14th Int. Conf. Ubiquitous Robots Ambient Intell.*, Jeju, South Korea, 2017, pp. 185–189.
- [5] C. Parrott, T. J. Dodd, and R. Groß, "HiGen: A high-speed genderless mechanical connection mechanism with single-sided disconnect for self-reconfigurable modular robots," *IEEE Int. Conf. Intell. Robots Syst.*, 2014, pp. 3926–3932.
- [6] W. Saab and P. Ben-Tzvi, "A genderless coupling mechanism with 6-DOF misalignment capability for modular self-reconfigurable robots," *J. Mech. Robot.*, vol. 8, no. c, pp. 1–9, 2016.
- [7] A. I. Nawroj, J. P. Swensen, and A. M. Dollar, "Toward modular active-cell robots (MACROs): SMA cell design and modeling of compliant, articulated meshes," *IEEE Trans. Robot.*, vol. 33, no. 4, pp. 796–806, Aug. 2017.
- [8] M. Pacheco, R. Fogh, H. H. Lund, and D. J. Christensen, "Fable II: Design of a modular robot for creative learning," in *Proc. IEEE Int. Conf. Robot. Autom.*, Seattle, WA, USA, May 2015, pp. 6134–6139.
- [9] J. Neubert, A. Rost, and H. Lipson, "Self-soldering connectors for modular robots," *IEEE Trans. Robot.*, vol. 30, no. 6, pp. 1344–1357, Dec. 2014.
- [10] R. F. M. Garcia, J. D. Hiller, K. Støy, and H. Lipson, "A vacuum-based bonding mechanism for modular robotics," *IEEE Trans. Robot.*, vol. 27, no. 5, pp. 876–890, Oct. 2011.
- [11] H. Ahmadzadeh, E. Masehian, and M. Asadpour, "Modular robotic systems: Characteristics and applications," *J. Intell. Robot. Syst.*, vol. 81, pp. 317–357, Mar. 2016.
- [12] J. Davey, N. Kwok, and M. Yim, "Emulating self-reconfigurable robots—Design of the SMORES system," in *Proc. IEEE/RSJ Int. Conf. Intell. Robots Syst.*, Oct. 2012, pp. 4464–4469.
- [13] J. W. Romanishin, K. Gilpin, S. Claiici, and D. Rus, "3D M-blocks: Self-reconfiguring robots capable of locomotion via pivoting in three dimensions," in *Proc. IEEE Int. Conf. Robot. Autom.*, 2015, pp. 1925–1932.
- [14] A. Brunete, A. Ranganath, S. Segovia, J. P. de Frutos, M. Hernando, and E. Gambao, "Current trends in reconfigurable modular robots design," *Int. J. Adv. Robot. Syst.*, vol. 14, May 2017, Art. no. 172988141771045.
- [15] T. Tosun, J. Davey, C. Liu, and M. Yim, "Design and characterization of the EP-Face connector," in *Proc. IEEE/RSJ Int. Conf. Intell. Robots Syst.*, Oct. 2016, vol. 19, pp. 45–51.
- [16] M. Yim, Y. Zhang, and D. Duff, "Modular robots," *IEEE Spectr.*, vol. 39, no. 2, pp. 30–34, Feb. 2002.
- [17] N. Eckenstein and M. Yim, "Modular robot connector area of acceptance from configuration space obstacles," in *Proc. IEEE/RSJ Int. Conf. Intell. Robots Syst.*, 2017, pp. 3550–3555.
- [18] E. A. Peraza-Hernandez, D. J. Hartl, R. J. Malak, Jr., and D. C. Lagoudas, "Origami-inspired active structures: A synthesis and review," *Smart Mater. Struct.*, vol. 23, Sep. 2014, Art. no. 094001.
- [19] A. Firouzeh and J. Paik, "Grasp mode and compliance control of an underactuated origami gripper using adjustable stiffness joints," *IEEE/ASME Trans. Mechatronics*, vol. 22, no. 5, pp. 2165–2173, Oct. 2017.
- [20] T. Yoshikai, M. Hayashi, A. Kadowaki, T. Goto, and M. Inaba, "Design and development of a humanoid with soft 3D-deformable sensor flesh and automatic recoverable mechanical overload protection mechanism," in *Proc. IEEE/RSJ Int. Conf. Intell. Robots Syst.*, Oct. 2009, pp. 4977–4983.
- [21] X. Guo *et al.*, "A torque limiter for safe joint applied to humanoid robots against falling damage," in *Proc. IEEE Int. Conf. Robot. Biomimetics*, Dec. 2015, pp. 2454–2459.